applied sciences

MDPI

Article

Intensity Prediction Equations Based on the Environmental Seismic Intensity (ESI-07) Scale: Application to Normal Fault Earthquakes

Marco Pizza [1,*], Francesca Ferrario [1], Alessandro M. Michetti [1,2], M. Magdalena Velázquez-Bucio [3], Pierre Lacan [3] and Sabina Porfido [2,4]

[1] Dipartimento di Scienza e Alta Tecnologia, Università degli Studi dell'Insubria, 22100 Como, Italy; francesca.ferrario@uninsubria.it (F.F.); alessandro.michetti@uninsubria.it (A.M.M.)
[2] Istituto Nazionale di Geofisica e Vulcanologia, Sez. Osservatorio Vesuviano, 80124 Naples, Italy; sabina.porfido@cnr.it
[3] Instituto de Geociencias, Universidad Nacional Autónoma de México, Juriquilla 76230, Mexico; magda_vb@yahoo.com.mx (M.M.V.-B.); placan@geociencias.unam.mx (P.L.)
[4] Consiglio Nazionale delle Ricerche-ISA, 83100 Avellino, Italy
* Correspondence: m.pizza@uninsubria.it

Abstract: Earthquake environmental effects may significantly contribute to the damage caused by seismic events; similar to ground motion, the environmental effects are globally stronger in the vicinity and decrease moving away from the epicenter or seismogenic source. To date, a single intensity prediction equation (IPE) has been proposed in the Italian Apennines for intensity scale dealings with environmental effects: the Environmental Seismic Intensity (ESI-07). Here, we evaluate the sensitivity of the IPE with respect to input data and methodological choices and we propose IPEs with global validity for crustal normal faults. We show the strong influence of input data on the obtained attenuation investigating the 1980 Irpinia–Basilicata (Southern Italy) earthquake. We exploit a dataset of 26 earthquakes to build an IPE considering the epicentral distance. We also propose an IPE considering the distance from the fault rupture, which is derived from a dataset of 10 earthquakes. The proposed equations are valid for normal faults up to 40 km from the epicenter/fault and may flank other models predicting ground motion or damage to the built environment. Our work thus contributes to the use of the ESI-07 scale for hazard purposes.

Keywords: intensity attenuation; ESI-07 scale; intensity prediction equations; earthquake; normal fault

Citation: Pizza, M.; Ferrario, F.; Michetti, A.M.; Velázquez-Bucio, M.M.; Lacan, P.; Porfido, S. Intensity Prediction Equations Based on the Environmental Seismic Intensity (ESI-07) Scale: Application to Normal Fault Earthquakes. *Appl. Sci.* **2024**, *14*, 8048. https://doi.org/10.3390/app14178048

Academic Editor: Nicholas Vassiliou Sarlis

Received: 8 August 2024
Revised: 31 August 2024
Accepted: 2 September 2024
Published: 9 September 2024

1. Introduction

Characterizing seismic hazards in regions where crustal faults can produce rare but powerful earthquakes is critical due to the potentially destructive nature of these events. To effectively characterize this hazard, it is essential to assess the intensity of earthquakes across different affected areas through intensity prediction equations (IPEs). For a consistent comparison between different geographic regions, here, we use an intensity scale based on the environmental effects caused by earthquakes, as this is not influenced by factors such as construction density, construction quality, or population perception.

Indeed, earthquakes generate significant effects on both anthropogenic and natural environments, which are the realm of intensity scales [1–3]. Slips along the seismogenic fault plane and ground shaking due to the propagation of the seismic wave are the main factors responsible for such effects. In such a context, attenuation models are fundamental to understand the attenuation mechanisms and, therefore, calculate the earthquake impact zones. These models are essential for any seismic hazard characterization and basically parametrize the decrease in intensity/ground motion with distance from the epicenter or seismogenic source [4]. Since the 1970s, thousands of ground motion prediction equations

have been published (e.g., [5,6]), predicting the expected level of Peak Ground Acceleration (PGA), Peak Ground Velocity (PGV), or Spectral Acceleration (SA). Regarding intensity, several tens of intensity prediction equations (IPEs) are available for different territorial settings [4,7–9], mostly based on the Mercalli–Cancani–Sieberg (MCS) intensity scale in Italy and on the Modified Mercalli (MM) scale worldwide. Ferrario et al. (2020) [10] introduced the first IPE based on the Environmental Seismic Intensity scale (ESI-07), a macroseismic scale where the Earthquakes Environmental Effects (EEEs) are the only descriptors [11–13].

In the last decades, several earthquakes have shown that EEEs are a relevant source of hazard, which may be even more prominent than ground shaking. Examples include the 2008 M_w 7.9 Wenchuan, China, the 2010 M_w 7.1 South Island, New Zealand, the 2011 M_w 9.0 Tohoku, Japan, and the 2023 M_w 7.8 and M_w 7.5 Turkey–Syria earthquakes [14–16]. Concurrently, in the last years, several initiatives were undertaken to develop high-resolution datasets of EEEs or in the systematic collection of such data (e.g., [17–20]). Furthermore, as demonstrated in specific studies, EEEs are considered good descriptors for the re-evaluation of historical earthquakes and, because of their homogeneous nature, can also be used for comparison between such earthquakes and modern ones (e.g., [21–23]).

The ESI-07 scale provides good objectivity in the assessment of macroseismic intensities, especially in the epicentral area, compared to traditional intensity scales influenced by human factors such as local economy, culture, and the enforcement of building seismic codes. Moreover, the ESI-07 scale does not saturate at high intensity levels and is independent of the location and distribution of settlements and the construction quality of buildings. Therefore, it enables the comparison of earthquake effects across different regions and time periods, which is crucial for hazard evaluation [24–26]. However, to date, only one IPE based on the ESI-07 scale has been proposed, and it is specific to a localized territorial setting (i.e., Ferrario et al., 2020, [10] in the Italian Apennines).

Here, we analyze and discuss the application of the ESI-07 scale for seismic hazard purposes. The aims of this article are three-fold:

1. Investigating the role of the resolution and uncertainty of the input data (e.g., number and accuracy of the EEE sites) and of methodological choices in the derivation of the ESI-07 IPE. This research addresses whether and how the quality and quantity of input data affect the final results. To this end, we analyzed a case study of the 1980 Irpinia–Basilicata, Southern Italy earthquake.
2. Evaluate the exportability of the IPE calculated in the Italian Apennines to other settings characterized by normal faulting. The objective is to determine whether this equation can be extended to achieve the first ESI-07-based IPE with global validity.
3. Proposing an ESI-07 IPE based on the distance from rupture rather than from the epicenter. Given that the strongest earthquakes can cause fault ruptures over tens of kilometers and that many IPEs are based on epicenter distance, this may lead to approximation errors in terms of distance. Therefore, we consider using the distance to rupture, aiming to calculate the first IPE based on the ESI-07 scale with this type of distance.

2. Intensity Attenuation: State of the Art and Definitions

Several IPEs are available in the literature, whose field of applicability depends on the dataset on which they are built. IPEs provide an estimation of expected intensity as a function of distance; available formulations differ in terms of the distance metric (e.g., distance from epicenter, hypocenter, rupture plane), adopted functional form, and methodological choices (e.g., input data, data censoring, statistical estimator).

Bakun and Wentworth (1997) [27] developed an IPE from a training set of 22 California earthquakes; their equation is computed as a function of distance from the macroseismic epicenter (MM scale) and adopted a linear functional form. Gasperini et al. (1999; 2010) [28,29] estimated the axial orientation, location of the seismogenic source, and earthquake size from macroseismic data in Italy. The epicenter location was calculated using the concept of macroseismic intensity attenuation as a function of distance. Bakun and Scotti (2006) [30] computed regional intensity attenuation models for 33 earthquakes in France, providing

region-specific coefficients. Ferrario et al. (2020) [10] calculated an IPE by analyzing 14 normal faulting earthquakes that occurred in Central and Southern Apennines (Italy) between 1688 and 2016; their equation adopts the epicentral distance and log-linear functional form.

The methodological aspects related to the derivation of IPEs are sketched in Figure 1. The map of the rupture area (Figure 1a) shows the epicenter (red star) and intensity data points (IDPs), which are all the points where EEEs have been observed and an ESI-07 value has been assigned. In this example, the earthquake generated a surface rupture along the principal and distributed faults (red segments) and other effects in the nearby region. Two ESI-07 hypothetical isoseismals, corresponding to intensities X (dotted blue line) and IX (dotted purple line), have been represented. The dotted black line is the trace of the main fault, intended as the rupture linework of the primary fault or tectonic/seismogenic feature responsible for the earthquake [19].

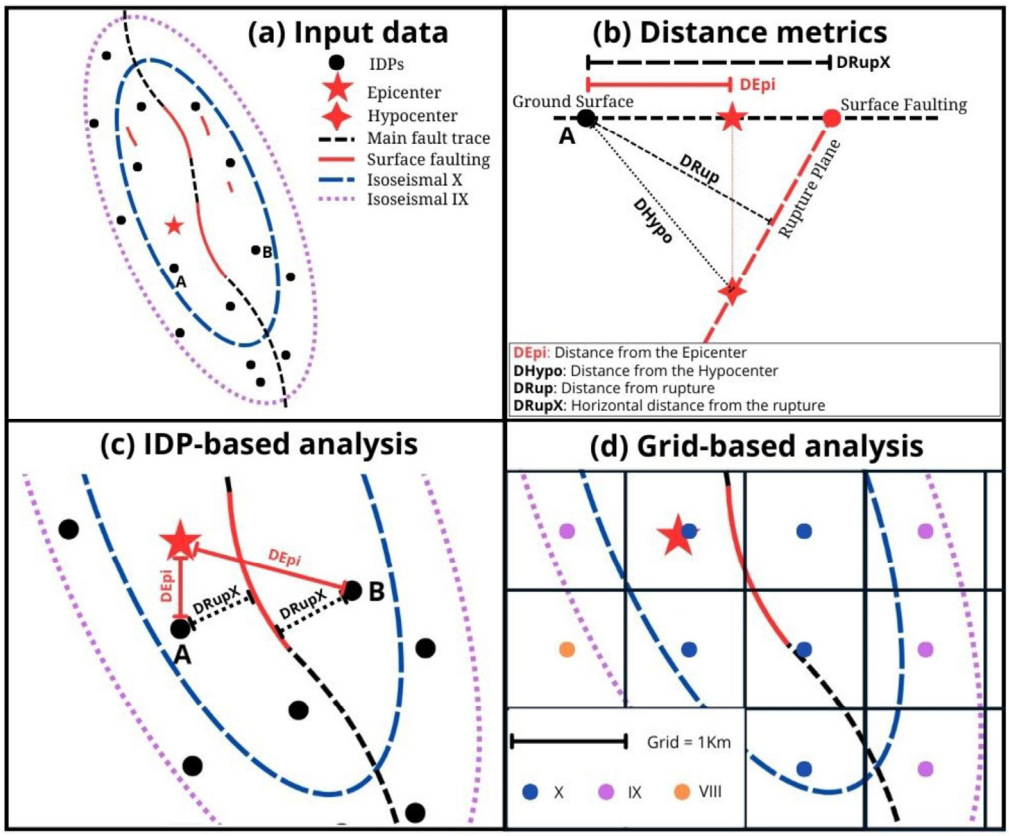

Figure 1. Sketch of the input parameters for IPE calculations: (**a**) map showing the surface faulting (red lines), epicenter (star), intensity data points (IDPs, black points), and isoseismal lines; (**b**) definition of horizontal distance from the rupture (D_{RupX}); (**c**) illustration of the epicentral distance (D_{Epi}) and distance from surface faulting (D_{RupX}), calculated with the IDP method; and (**d**) grid method (the values shown in the figures are only an example and do not refer to any specific case).

The different ways to compute the source-to-site distance for a normal fault are represented in Figure 1b: D_{Epi} represents the distance from the epicenter (adopted, for instance, by Bakun and Wentworth, 1997; Ferrario et al., 2020 [10,27]); D_{Hypo} is the distance from the hypocenter (i.e., Gasperini, 2001; Albarello and D'Amico, 2004 [31,32]); D_{Rup} is the distance from the fault rupture [33,34]; and finally, D_{RupX} is the closest horizontal distance between each IDP and the main fault rupture.

IPEs can be derived using point-based (Figure 1c; e.g., Bakun and Wenthworth, 1997, Ferrario et al., 2020 [10,27]) and grid-based approaches (Figure 1d; e.g., Chunga et al., 2018 [35]). The former requires the availability of point data, while the latter requires the availability of isoseismals. In the IDP-based analysis, each point (A and B in the example)

is labeled with the intensity and distance values; then, data are analyzed statistically. In the grid-based analysis, firstly, a grid of cells of a given dimension (1 km^2 in the example) is created and the cell center is extracted. The corresponding ESI-07 value is assigned to each cell according to the isoseismal value; distance values are assigned too. In this manner, the territory is systematically sampled, reducing the bias of inhomogeneous IDP locations. On the contrary, the grid-based approach relies on isoseismals, whose delineation may be more subjective than in single IDP intensity assessments.

In the following, we explore the impact of different methodological choices (i.e., IDP-based vs. grid-based approaches) on the computation of the intensity–distance attenuation.

3. Data and Methods

3.1. Aim 1: Role of Input Data and Methodological Choices

Figure 2 presents the methodological workflow, referring to the three aims of the work outlined above. To analyze the role of the quality and quantity of the input data, we selected a case study of the 1980 M_w 6.8 Irpinia–Basilicata, Southern Italy earthquake [36]. This earthquake was already included in the analyses conducted by Ferrario et al. (2020) [10], but here we enlarged the number of available data points from 66 [37] to 563, thanks to a careful review of the published data, analysis of technical reports and administrative documents, and interviews of eyewitnesses, supplemented with field surveys at selected sites [38]. Additionally, we derived original ESI-07 isoseismals, which were not available to date.

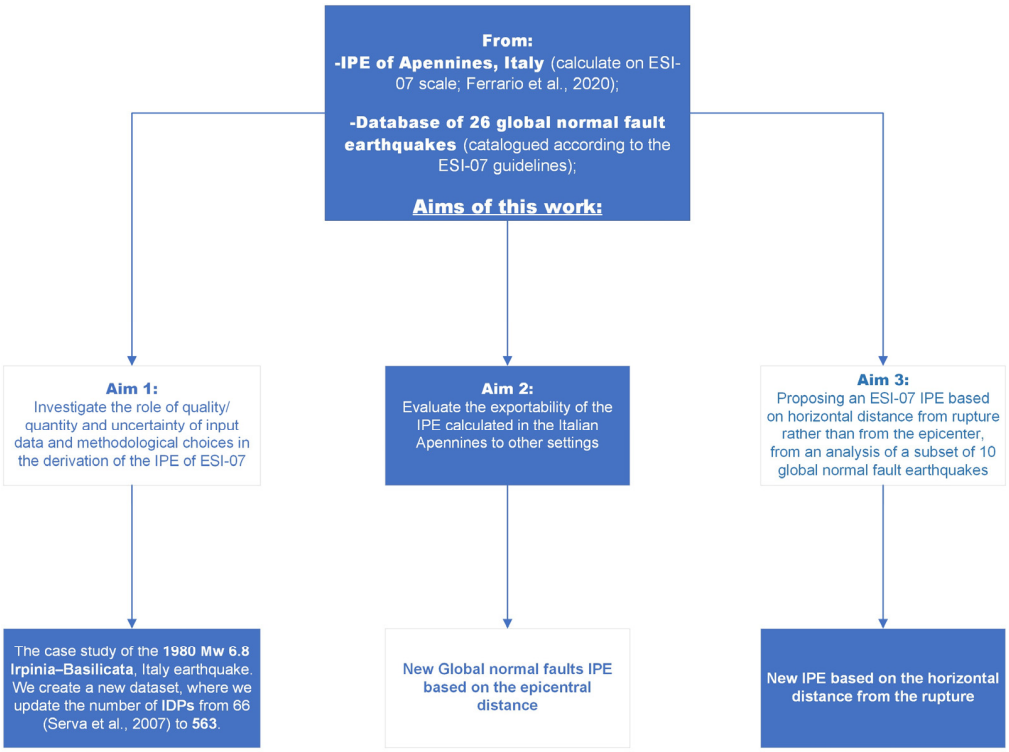

Figure 2. Methodological workflow adopted in the current study [10,37].

We evaluated the influence of several methodological choices in the derivation of an intensity prediction equation. We considered three different input datasets: "previous" IDPs (from Serva et al., 2007 [37]), "new" IDPs, and ESI-07 isoseismals, analyzed on a 1-kilometer grid (from Pizza et al., 2023 [38]). Starting from the analysis of all IDPs, we calculated the median distance for each intensity class and investigated the results in terms of the intensity–distance attenuation.

3.2. Aim 2: Normal Faulting IPE with Global Validity (Epicentral Distance)

We addressed the second issue, the exportability of the Italian Apennine IPE to other settings by collecting a dataset of normal faulting earthquakes with available IDPs (Table 1). We applied the same method of Ferrario et al. (2020) [10] to derive an updated IPE valid on a global scale: the attenuation was computed from the IDPs, employing the "intensity binning" methodology introduced by Bakun and Wentworth (1997) [27] and considering the median epicentral distance of each intensity class.

Table 1. Summary of the events investigated in this study; in bold we highlight the case histories used for the analysis of the intensity attenuation with distance from the fault; the N° n. IDPs refer to those resulting after data decimation.

Event	Country	Date	Lat.	Long.	Magnitude	ESI-07 I_0	N° IDPs	Ref. ESI-07 Data
Sannio	Italy	5 June 1688	41.28	14.56	7.1	X	11	[37]
Avola	Italy	11 January 1693	37.12	14.93	7.4	X	4	[39]
Irpinia–Basilicata	Italy	8 September 1694	40.86	15.41	6.7	X	6	[37]
Norcia	Italy	14 January 1703	42.71	13.07	6.8	X	4	[39]
L'Aquila	Italy	2 February 1703	42.43	13.29	6.6	X	7	[39]
Puglia	Italy	20 February 1743	39.85	18.77	7.1	XI	2	[40]
Estubeny	Spain	23 March 1748	39.03	−0.63	6.2	IX	32	[41]
Calabria	Italy	5 February 1783	38.30	15.97	7.1	XI	34	[42]
Molise	Italy	26 July 1805	41.50	14.47	6.7	X	38	[37]
Basilicata	Italy	16 December 1857	40.35	15.84	7.1	X	41	[39]
Atalanti	Greece	27 April 1894	38.63	23.10	6.8	X	19	[43]
Messina	Italy	28 December 1908	38.15	15.69	7.1	XI	59	[44]
Acambay	Mexico	19 November 1912	19.98	−99.83	6.9	X	54	[45]
Fucino	Italy	13 January 1915	42.01	13.53	7.1	X	9	[39]
Irpinia	Italy	23 July 1930	41.07	15.32	6.7	X	29	[37]
Sofades	Greece	30 April 1954	39.28	22.29	6.8	IX-X	6	[46]
Albolote	Spain	19 April 1956	37.15	−3.39	5.4	VIII	8	[47]
Thessaloniki	Greece	20 June 1978	40.70	23.30	6.5	IX	22	[43]
Irpinia	Italy	23 November 1980	40.84	15.28	6.9	X	534	[38]
Kalamata	Greece	13 September 1986	37.11	22.14	6.1	IX	51	[48]
Pyrgos	Greece	26 March 1993	37.68	21.46	5.7	VII-VIII	7	[26]
Kozani	Greece	13 May 1995	40.16	21.68	6.5	IX	19	[43]
Colfiorito	Italy	26 September 1997	43.01	12.85	6.0	IX	23	[39]
L'Aquila	Italy	6 April 2009	42.31	13.51	6.3	IX	27	[39]
Amatrice	Italy	24 August 2016	42.70	13.23	6.2	IX	14	[10]
Samos	Greece	30 October 2020	37.76	26.81	7.0	IX	46	[49]

Prior to computing the attenuation relations, data were decimated to avoid the incompleteness bias in the far field. We adopted the method described by Gasperini (2001; Equation (1)) [31] and already used in Ferrario et al. (2020) [10], building a preliminary attenuation to estimate the distance at which the intensity falls below a given threshold, which here, was set to ESI-07 $\geq$ V.

Using all the IDPs contained in the dataset, we calculated the median distance for each intensity class. The median distance for the threshold value of ESI-07 = V was determined to be 65 km. Accordingly, we excluded all data points with distances exceeding this value. Data points corresponding to half-degrees were also removed.

Considering that the analyzed earthquakes have different epicentral intensities (I_0), we used ΔI [31] to calculate an IPE for the entire dataset:

$$\Delta I = I_0 - I_i \quad (1)$$

where I_0 is the epicentral intensity and I_i is the local intensity assigned to the "ith" site.

According to Ferrario et al. (2020; Equation (2)) [10], we adopted a log-linear functional form, defined as follows:

$$\Delta I = a + b \times \log_{10}(R) + c \times R \quad (2)$$

where R is the epicentral distance (in km), and a, b, and c are fitting coefficients.

3.3. Aim 3: Normal Faulting IPE (Distance from Fault)

Finally, we developed an IPE based on the horizontal distance from the surface rupture on a subset of earthquakes, i.e., those with reliable information on the primary surface faulting location (highlighted in bold in Table 1). The methodology was similar to the one adopted for "Aim 2", however in this case, attenuation was defined by the minimum horizontal distance (D_{RupX}) between each IDP and the main fault rupture (Figure 1). The IDPs used for this analysis are those retained after the data decimation process. For small to moderate earthquakes, the point-source approximation is often considered; however, for large earthquakes, this assumption is no longer valid and the distance from the fault plane is preferable. This requires a good knowledge of the fault architecture at depth (e.g., dip angle, non-planar surfaces), which in our dataset was lacking, especially for older events. Since surface faulting is an environmental effect of paramount importance, it is usually recorded in ESI-07 studies, thus we chose the D_{RupX} as the distance descriptor.

4. Results

4.1. Update of the 1980 Irpinia–Basilicata Dataset

To reach the first aim of this work, we created a new dataset [38], where we updated the number of IDPs for the 1980 Irpinia–Basilicata earthquake, moving from 66 [37] to 563 IDPs. Figure 3 shows the spatial distribution of the IDPs, color-coded according to the type of effect, and the ESI-07 isoseismals. Most of the effects are located in the epicentral area: 56.9% are within 20 km of the macroseismic epicenter (40.842 N, 15.283 E; [36]) and 84.4% are within 40 km; however, some effects were located nearly 200 km from the epicenter. The area with severe effects (I = X ESI-07) covers about 200 km^2; if we consider the area included in isoseismal VIII ESI-07, it covers about 2000 km^2.

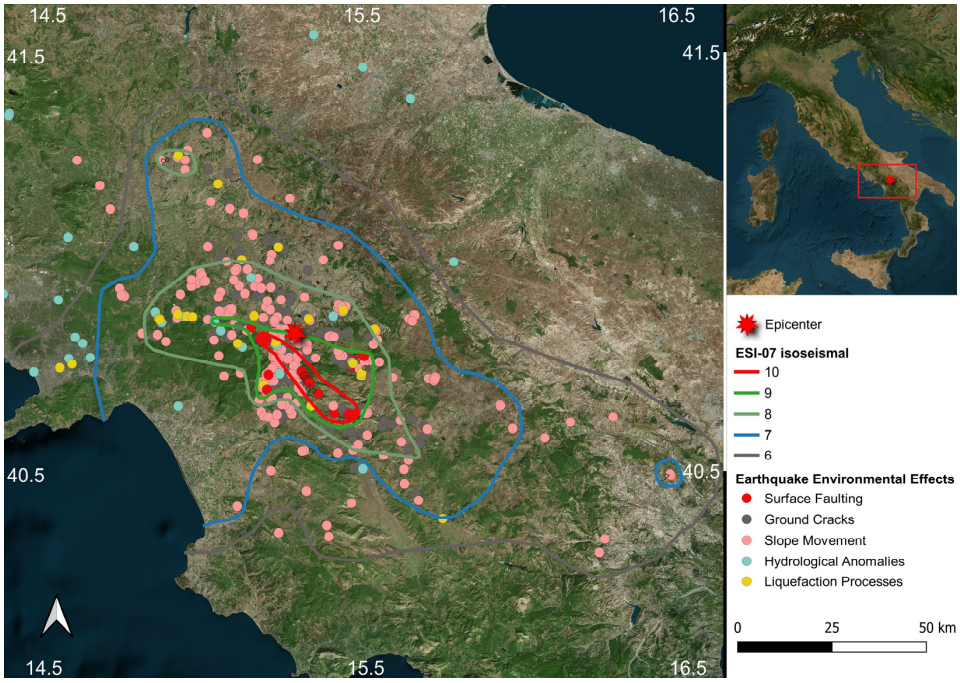

Figure 3. Location of IDPs contained in the new dataset, and ESI-07 isoseismals, referring to the 1980 Irpinia–Basilicata, Southern Italy earthquake.

We explored the intensity attenuation using different data inputs, namely, (i) the dataset introduced by Serva et al. (2007) [37], (ii) the "new" database [38], and (iii) the ESI-07 isoseismals originally drawn in the current research. The first two datasets were analyzed using the IDP method, while the third dataset was analyzed using the grid method.

As shown in Table 2, the dataset realized by Serva et al. (2007) [37] includes 66 IDPs, the "new" dataset contains 563 IDPs, and the grid-based dataset derived from the isoseismals includes 12,634 data points.

Figure 4a shows the new IDPs (orange dots) and the median epicentral distance calculated for each intensity class. The new dataset shows a considerable increase in the number of IDPs over the entire intensity range (Table 2), with particular reference to the points documented within 40 km from the epicenter. In Figure 4b, we provide the median distances for each ESI-07 degree obtained from the three Irpinia–Basilicata datasets (open symbols);, the black line is the reference IPE for the Apennines derived after Ferrario et al. (2020) [10] considering an epicentral intensity of ESI-07 X.

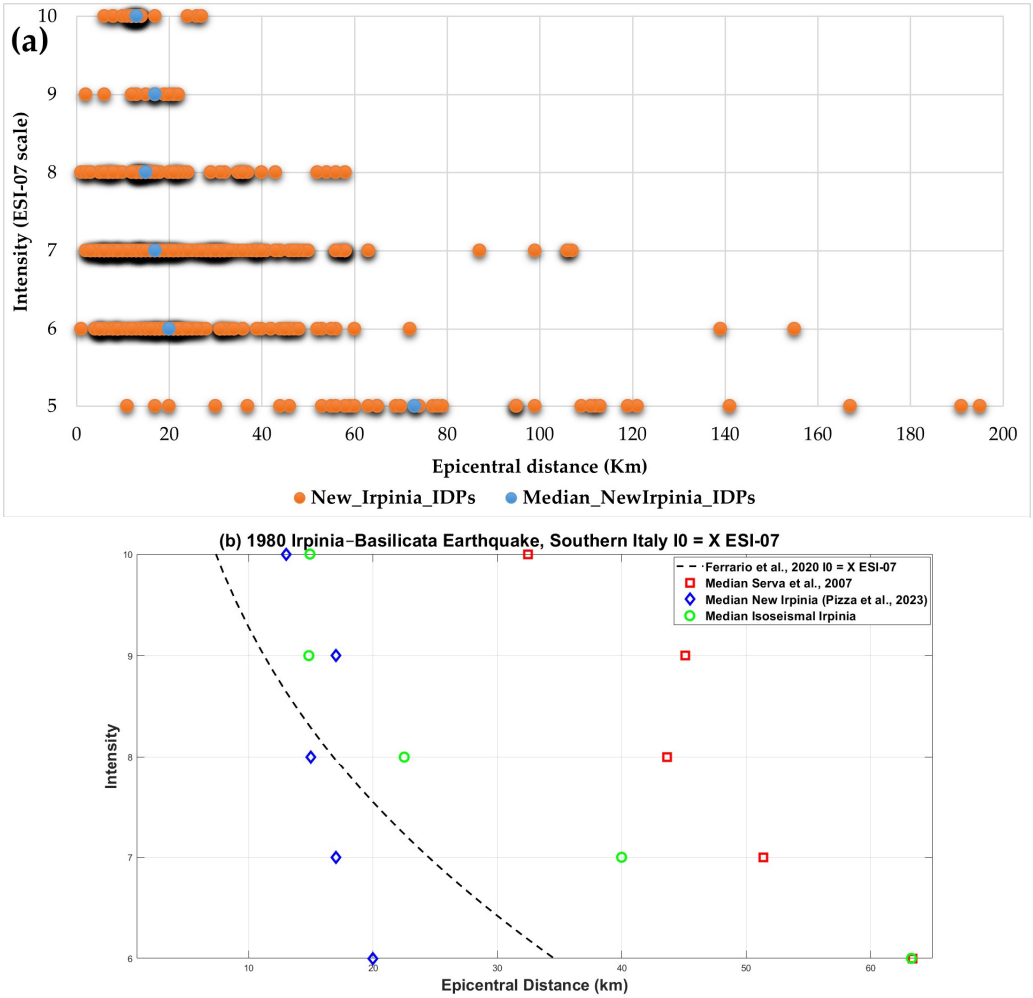

Figure 4. (**a**) IDPs and their relative medians from the "new" 1980 Irpinia–Basilicata dataset; (**b**) ESI-07 attenuation of each analyzed dataset compared to the reference IPE for the Apennines, Italy, calculated by Ferrario et al. (2020) [10] and [37,38].

Figure 4b shows that the quality of the input data significantly affects the final output. We recall that the purpose here is to explore the methodological issues and not to derive an IPE specific for the 1980 Irpinia–Basilicata earthquake. When examining the database created by Serva et al. (2007) [37], the median values for each intensity level were higher than those calculated using the new dataset and through isoseismal maps. These differences can

be attributed to the total number of intensity data points (IDPs) analyzed and their spatial distribution. The new database [38] has lower values compared to the previous [37] and the isoseismal-derived databases. Specifically, the new database has a higher percentage of points in the near field (within 15 km), 40% compared to 5% for "Isoseismal Irpinia", and none for Serva et al. (2007) [37].

Table 2. Number of observations and median epicentral distances for the 1980 Irpinia–Basilicata earthquake.

	1980 Irpinia–Basilicata, Italy	ESI-07 VI	ESI-07 VII	ESI-07 VIII	ESI-07 IX	ESI-07 X
Nr. Observations	IDP Serva et al., 2007 [37]	4	20	35	4	2
	IDP Pizza et al., 2023 [38]	137	248	89	14	38
	Isoseismals	6017	4581	1444	404	188
Median distance (km)	IDP Serva et al., 2007 [37]	63	51	44	45	32
	IDP Pizza et al., 2023 [38]	20	17	15	17	13
	Isoseismals	63	40	23	15	15
	Predicted (Ferrario et al., 2020 [10], assuming I_0 = X)	35	24	17	11	7

4.2. Deriving an ESI-07 IPE for Normal Faulting Earthquakes with Global Validity

To derive an IPE with global validity for normal faulting earthquakes, we built a dataset (Table 1) of 26 global earthquakes that occurred between 1688 and 2020. The selected earthquakes (magnitude range 5.4–7.4) occurred in Italy, Greece, Spain, and Mexico and have an ESI-07 I_0 within the range of IX to XI. The distribution of data, in relation to ESI-07 intensity, shows a Gaussian-type distribution, with about 70% of the data between ESI-07 VI and VIII (Figure 5a). Following the data decimation process, our dataset encompasses a total of 1106 intensity data points (Figure 5b); 48% of the IDPs are located within 15 km from the epicenter and 91% within 40 km.

In Figure 6a, we introduce the intensity prediction equation developed using the new global dataset, expressed in terms of ΔI versus epicentral distance; the curve and 95% confidence bounds are shown; numerical coefficients are presented in Table 3. The attenuation is steeper in the range between about 10 and 25 km, then gradually decreases.

Table 3. Summary of the results obtained in terms of "epicentral distance" (D_{Epi}) and "horizontal distance from the fault" (D_{RupX}). SSE: Sum of Squared Errors, RMSE: Root Mean Square Error.

Log-Linear Model: $R = a + b \times \log_{10}(R) + c \times R$, where R is the Distance (km):							
Type of Distance (R)	**a (95% Conf. Bounds)**	**b (95%)**	**c (95%)**	**SSE**	**R^2**	**Adj. R^2**	**RMSE**
D_{Epi}	−16.14 (−31.15, −1.128)	17.81 (1.406, 34.21)	−0.183 (−0.4639, 0.09788)	0.9941	0.9432	0.9053	0.5756
D_{RupX}	1.167 (−0.5689, 2.903)	0.8557 (−0.8146, 2.526)	0.06127 (−0.06005, 0.1826)	2.846	0.8374	0.7289	0.974

In Figure 6b, we draw the curves of the expected ESI-07, considering the I_0 values of XI, X, and IX; solid lines represent the results obtained in this study while dashed lines are the same using the equation of Ferrario et al. (2020) [10]. This comparison provides insights into the consistency and reliability of our proposed IPE equation. Figure 6b shows that the slope of the IPE derived in this study using epicentral distance is more pronounced than the one developed by Ferrario et al. (2020) [10], resulting in a faster attenuation. Nevertheless, the two equations are fairly similar since the difference between the two is generally within one degree of intensity (Figure 6c).

Given the distribution of the input data, we consider the proposed equation reliable up to 40 km, and we do not recommend extrapolation beyond these limits.

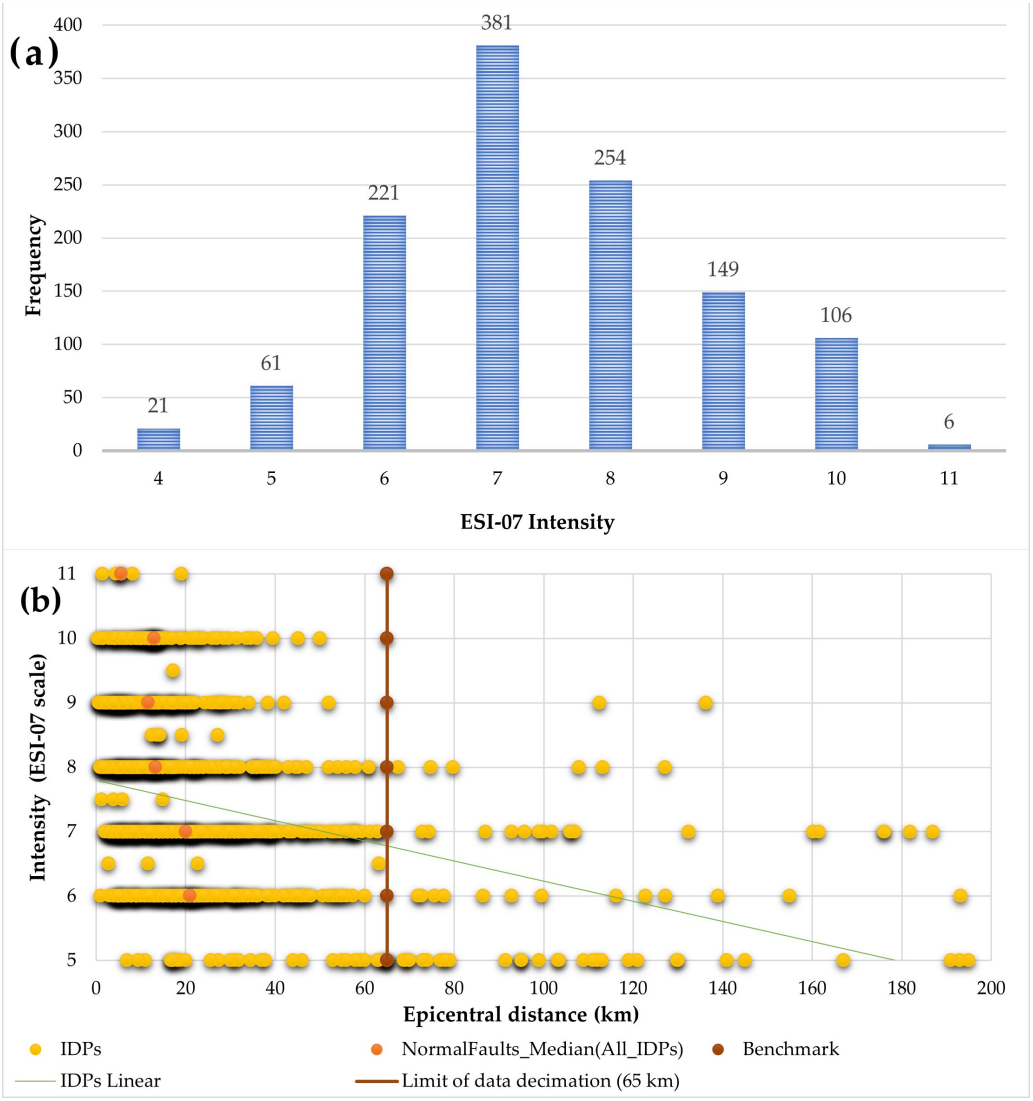

Figure 5. Distribution of the intensity data points (IDPs) in terms of (**a**) intensity (ESI-07 scale) and (**b**) epicentral distance (km). The red line represents the limit of the data decimation (65 km).

4.3. Attenuation with Distance from Fault Rupture

Measuring distances from the epicenter or hypocenter, as conducted for "Aim 2" of this work, can be an oversimplification in the case of strong earthquakes, when the point-source approximation is no longer valid. Figure 7 shows two examples of earthquakes included in our dataset, namely the 1894 Atalanti, Greece and 1912 Acambay, Mexico events. The surface rupture length along the main fault is 36 km for Acambay [50,51] and 32 km for Atalanti [52]. IDPs are not distributed uniformly in space; in fact, especially for Atalanti, most of them are located near the fault. Therefore, using the epicentral distance might generate an error in the order of even tens of kilometers, while using a different distance metric, such as from the fault, will reduce this error. Many studies use the distance from the seismogenic plane at depth, or the Joyner–Boore distance; numerical equations to relate the different distance measures have been proposed as well [33]. Due to the paucity of such information for the earthquakes in our dataset, we rely on the horizontal distance from the rupture (D_{RupX}, see Figure 2b), which we consider better constrained in studies dealing with the ESI-07 scale.

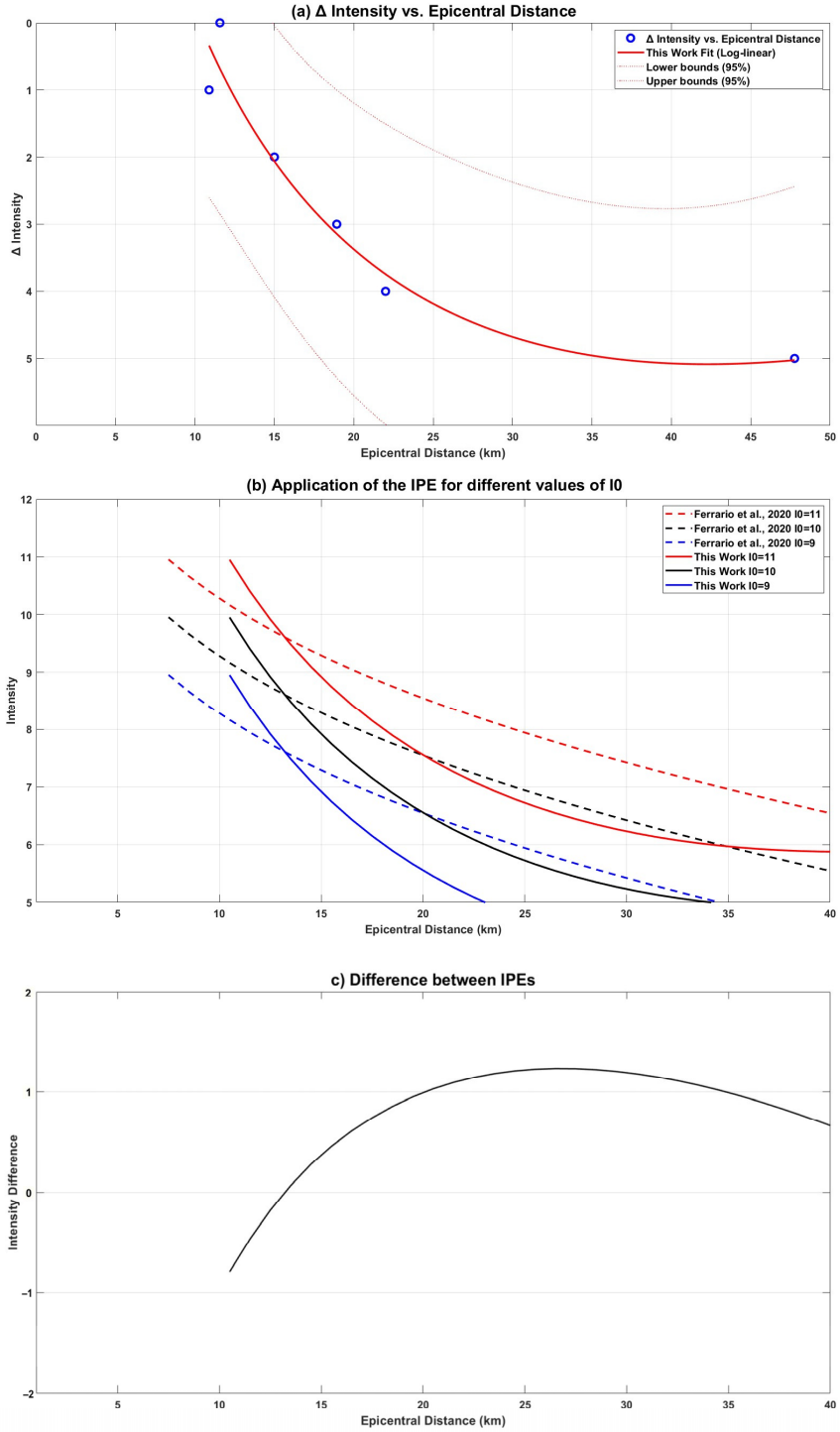

Figure 6. (**a**) Representation of IDP median values obtained from intensity binning, and the proposed ESI-07 IPE (with confidence bounds of 95%); (**b**) expected ESI-07 values considering various I_0, where the solid lines refer to the equation derived in this study and dashed lines are after Ferrario et al. (2020) [10]; (**c**) difference between IPEs (Ferrario et al., 2020 [10] minus the curve derived in this work).

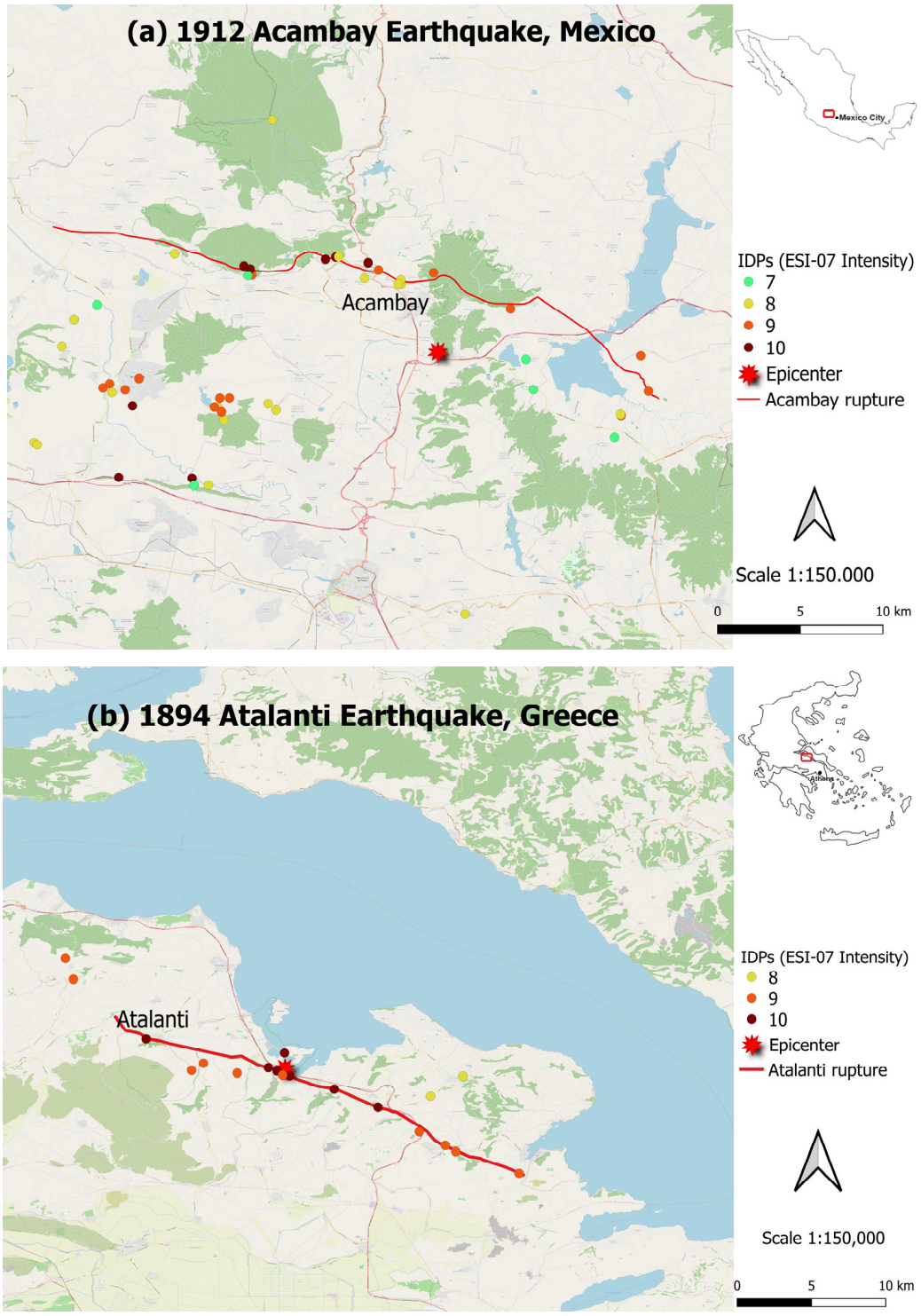

Figure 7. Examples of IDP maps referring to (**a**) 1912 Acambay earthquake, Mexico (IDPs from Velázquez-Bucio et al., 2024 [45]; surface rupture from Langridge et al., 2000 [50]); and (**b**) 1894 Atalanti earthquake, Greece (IDPs from Papanikolaou and Melaki, 2017 [43]; surface rupture from Pantosti et al., 2001 [52]).

After the data decimation process, our analysis focused on 726 IDPs. Each earthquake's rupture was delineated end-to-end through the reference literature [46,50,52–59]. The new IPE was computed by employing an approach consistent with that used in Aim 2 (i.e., IPE relative to epicentral distance). This process ensures the comparability of our findings.

Figure 8 presents the new IPE based on the horizontal distance from the rupture (D_{RupX}); numerical coefficients are provided in Table 3. The median value of ΔI = 0 is located within 1 km of the fault, while considering a ΔI between 1 and 4, a marked attenuation trend can be observed in the interval between about 10 and 15 km. The trend then smooths out, similar to what is observed for the epicentral distance. In fact, the median value of ΔI = 5 is located at almost 43 km.

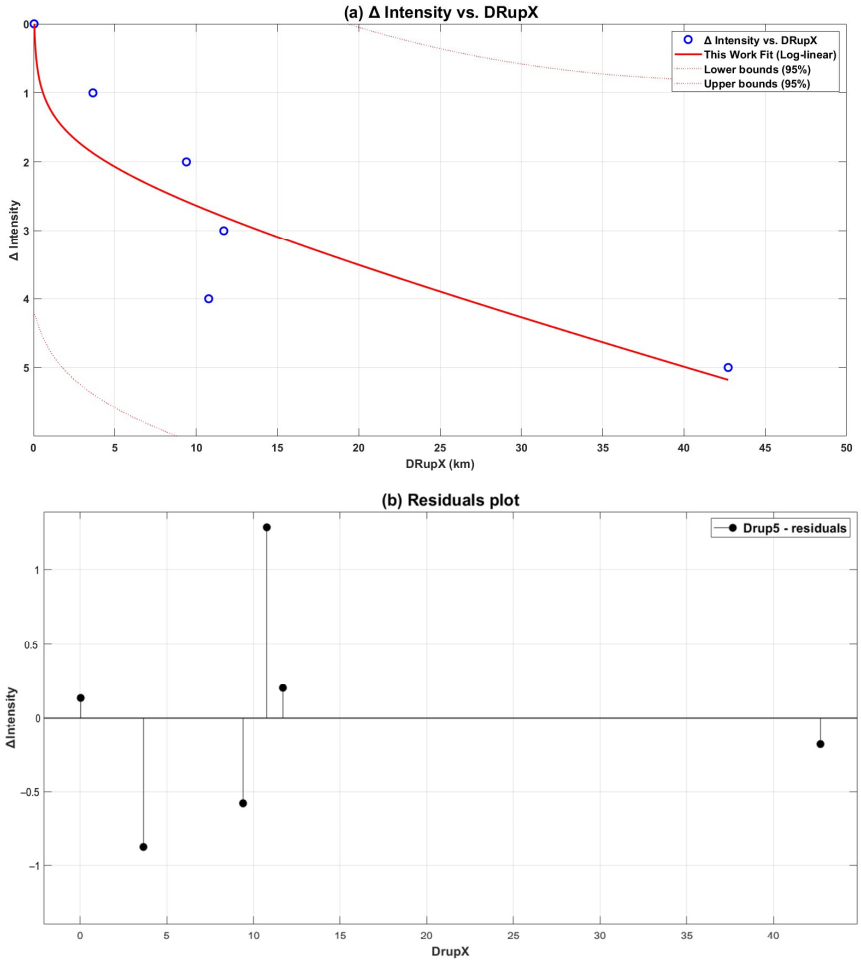

Figure 8. (**a**) Representation of IDP median values obtained from intensity binning, and the proposed IPE based on the horizontal distance from the rupture, D_{RupX} (with confidence bounds of 95%); (**b**) residual plot of the data (IDPs) analyzed in this work.

5. Discussion

In order to calculate the new intensity prediction equation (IPE), it is crucial to analyze the role of input data. The data quality and quantity significantly influence the final result, emphasizing the relevance of the data collection phase. For instance, the new database on the environmental effects of the 1980 Irpinia–Basilicata earthquake [38] exemplifies the importance of enhancing the quantity and quality of available data. This database allows for a detailed examination of the spatial distribution of intensity levels across the affected region, providing valuable, spatially continuous, and homogeneous insights into the impact of the earthquake. As illustrated in Figure 4b, the final output, in terms of attenuation, based on this new database, markedly differs from previous data inputs [37]. Several factors contribute to this difference. Notably, datasets with fewer points tend to highlight "maximum" effects over "typical" effects. While this approach is beneficial for a conservative analysis, it obscures details on "average" versus "giant" values [60]. Given that IPEs and GMPEs (Ground Motion Prediction Equations) are foundational for hazard maps and scenario definitions, it is essential to determine whether input parameters are

based on average or maximum values. For lower degrees of intensity, such as I = V or VI ESI-07, data incompleteness bias at large distances is often cited. However, this bias can also occur at short distances; for instance, focusing solely on the strongest effects in the epicenter area neglects lower intensity effects at short distances. Consequently, if data quality or quantity are compromised in the far field, the median distance decreases, whereas if this occurs in the near field, the median distance increases. This observation explains the findings related to "Aim 1" of this work (Figure 4b). Observing the blue points that represent the median intensity values, the new 1980 Irpinia–Basilicata dataset exhibits steeper attenuation due to the abundance of ESI-07 V-VI points at short distances. This scenario underscores the importance of evaluating the minimum intensity threshold to consider the data as reliable. The choice on the minimum ESI-07 threshold impacts the number of ΔI classes available for regression purposes; in this study, we set this threshold to ESI-07 $\geq$ V, which we consider as the best compromise between data quality/availability and statistical rigor.

In order to obtain large datasets and compare events in various seismotectonic and climatic settings, it is important to build standardized datasets. Several efforts have been recently realized for surface ruptures and earthquake-induced landslides [20,61]. However, currently, these data (i) refer to a single environmental effect at a time and (ii) have no ESI-07 information. A future prospect could be to create an integrated dataset on all the environmental effects induced by an earthquake, similar to what is implemented in the Earthquake Environmental Effects Catalogue [39].

Moreover, Figure 4b shows that methodological choices can also influence the final result. The data obtained from the new 1980 Irpinia–Basilicata database revealed a marked difference between the values derived from the IDP-based method and those calculated using the grid-based method. This discrepancy can be attributed to the fact that the IDP-based method has fewer values at large distances and that delineating isoseismals using the grid-based method may involve a more subjective component compared to evaluating the intensity of individual IDPs.

Consequently, this work demonstrates that the quality of the input data has a more significant impact on the final output than the statistical and methodological choices used for fitting the data.

Additionally, it is important to consider that most of the intensity prediction equations (IPEs) currently available were developed several years ago. This implies the need for systematic updates of these equations over time. For example, in the Italian geological context, these equations generally predate the significant seismic events of 2009 in L'Aquila and 2016 in Central Italy [31,32,62–65]. These equations usually refer to the MCS scale and adopt hypocentral or epicentral distances.

An update was proposed by Gomez-Capera et al. (2024) [66], who developed attenuation models specific to Italy. These models are calibrated in terms of magnitude (M_w) and are based on an empirical relationship between macroseismic intensity and energy. This study, based on post-1900 Italian earthquakes, uses the hypocentral distance as a descriptor.

Since its inception, the ESI-07 scale has been immediately considered for the analyses of macroseismic attenuation models due to its ease of use and its ability to provide homogeneous data across both historical and recent earthquakes, allowing for comparative analyses [26,43]. However, to date, only one IPE based on the ESI-07 scale has been proposed, calculated specifically for the Apennines region of Italy [10].

Indeed, this work aims, on the one hand, to update the existing IPEs and, on the other hand, to further explore the use of the ESI-07 scale for hazard purposes. Analyzing the D_{Epi}-based IPE, Figure 6b,c shows that comparing the attenuation relationship we obtained with that calculated by Ferrario et al. (2020) [10], the attenuation trend is similar, but the curve calculated in this study has a steeper slope.

These results, and consequently the differences with the attenuation calculated by Ferrario et al. (2020) [10], can be explained by the epistemic uncertainty, the input data, and the nature of intensity scales themselves. Certainly, it is possible to refer to the quality

of the input data but also to a component of uncertainty related to macroseismic scales. Indeed, these observations can be influenced by various factors and uncertainties, such as cumulative effects and the overlap of effects across different degrees, leading to a certain level of disparity between the theoretical expectations and observed realities due to assumptions and subjective evaluations of the researchers [67].

Another possible explanation relates to the data's spatial distribution. The majority of IDPs are located in the epicenter area or, at most, within a few tens of kilometers from it (74% within 25 km). This is because larger effects are more easily catalogued than smaller ones, and the ESI-07 scale is not entirely accurate in describing effects located in the far field [26,60]. Additionally, the level of urbanization in the earthquake-affected area is significant; although the ESI-07 scale is unrelated to the anthropogenic environment, the lack of a population in certain areas, especially in the far field, can result in not observing any effects, particularly those of lower intensity. In this research, we analyzed countries with different population densities, with the consequence that this parameter may have partly affected the final number of IDPs available for each earthquake. Indeed, i.e., Italy, analyzed by Ferrario et al. (2020) [10], nowadays has a significantly higher density, compared to Spain, Greece, and Mexico.

Additionally, the local geology can contribute to these differences, actively influencing the spatial distribution of the seismo-induced effects. The geological, geomechanical, and morphological characteristics of a site can attenuate or amplify earthquake effects. Consequently, there may be minimal effects or intensities lower than expected in areas near the epicenter, while significant effects may occur in the far field.

D_{RupX} was developed to introduce an easily identifiable and replicable distance from the fault, applicable to both historical and recent earthquakes. To ensure the effectiveness of the IPEs, it is necessary to maintain consistency between historical data and recent earthquake data.

We further assess the influence of the statistical data treatment, specifically targeting lower intensity values, by exploring different data censoring, both for D_{Epi} and D_{RupX}. Indeed, we test a fit considering values up to $\Delta I = 5$, or up to $\Delta I = 4$. As shown in Figure 9, considering or neglecting the data point at $\Delta I = 5$ has a tremendous influence on the attenuation, for both D_{RupX} and D_{Epi}. When neglecting the points at $\Delta I = 5$, the attenuation is significantly steeper; using the log-linear fit, the difference becomes particularly pronounced after 25 km for D_{Epi} and after 10 km for D_{RupX}. Figure 9 thus shows that the user choice of data censoring has a much more relevant effect than the choice of using distance from the epicenter or from the rupture. Our preferred curve is the one retaining the $\Delta I = 5$ data points (Table 3), since we consider them reliable enough for the case histories analyzed in this research; however, we encourage the user to carefully evaluate the feasibility of this choice for their specific case, or eventually handle uncertainty considering different model parametrizations.

The faster attenuation observed in the D_{RupX}-based IPE can be explained by the fact that stronger effects are generally the primary ones. Surface faulting, the most impactful of primary environmental effects, is certainly located on the primary fault, and eventually on other nearby structures. Indeed, the median for $\Delta I = 0$ is almost directly on the fault (0.03 km). Additionally, it is important to consider that for strong earthquakes, the surface rupture length may be of several tens of kilometers [68]. Therefore, considering that the epicenter is a single point, some IDPs may be located tens of kilometers away from it, while still being close to the seismogenic source. On the other hand, D_{RupX} serves as a better descriptor of the relationship between the localization of the EEEs and the seismogenic source itself.

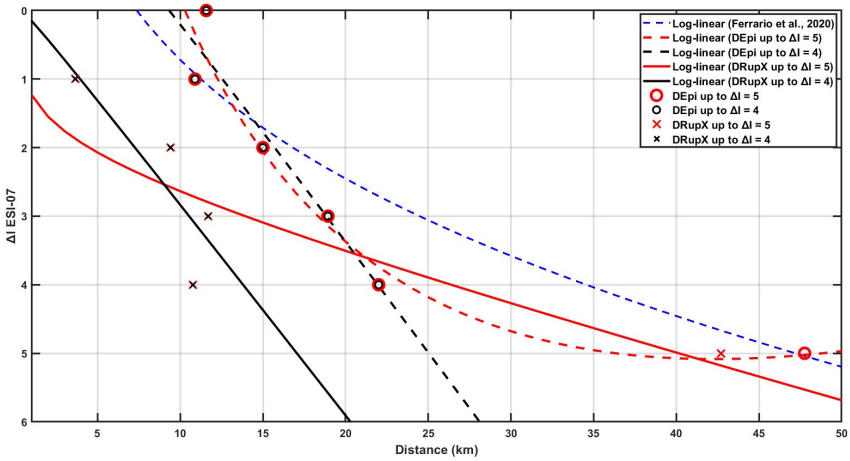

Figure 9. Representation of the proposed new IPEs: those based on D_{Epi} and D_{RupX} up to ΔI = 5 are shown in red, while those up to ΔI = 4 are shown in black. The trend was derived using a log-linear fit [10].

6. Conclusions

In this study, we calculated two new IPEs based on the ESI-07 scale, specifically for onshore normal fault earthquakes in the 5.4–7.4 M_w range. First, we calculated the D_{Epi}-based IPE using a dataset of 26 global earthquakes and employing the epicentral distance. Subsequently, we calculated the D_{RupX}-based IPE using a subset of 10 earthquakes, which generated surface rupture, from the same dataset. In both cases, we employed the IDP-based analysis methodology. Additionally, we analyzed the influence of the input data on the final results, with particular reference to the 1980 Irpinia–Basilicata earthquake.

The use of macroseismic intensity as a parameter for seismic hazard is widely accepted internationally, with many countries evaluating hazards exclusively in terms of intensity [69]. Seismic hazard maps are generally correlated with the predicted intensity at a site and its attenuation with distance. The ESI-07 scale has already been identified as a useful tool for hazard assessment (e.g., [70]), thus we consider it appropriate to implement IPEs based on this scale. The chosen methodology is easily replicable, and alongside the widely used D_{Epi}, we include D_{RupX}, a distance that can be easily calculated for both historical and recent earthquakes provided that they generate surface faulting. It is important to remark that the ESI-07 scale has good assets to calculate the attenuation or to complete the results calculated with other macroseismic scales. Therefore, this research aims to provide an additional contribution to the calculation of new IPEs, with the goal of improving our knowledge of seismic hazards in specific contexts.

Among the limitations of this approach is the applicability of the new IPEs, which is limited to a few tens of kilometers from the epicenter/fault. This limitation is due to the fact that the ESI-07 scale offers a certain reliability in the process of assessing macroseismic intensities in the epicentral area, while it tends not to accurately describe such values in the far field [26]. Indeed, we consider the proposed equations reliable up to 40 km and do not recommend extrapolation beyond these limits. Additionally, the proposed IPEs are valid for normal faults only, given the wider availability of ESI-07 data for such settings.

We believe that the development of ESI-07-based IPEs can be further refined and improved. Among future prospects, we consider the development of new IPEs based on 3D D_{Rup}, i.e., the distance perpendicular to the fault plane, the analysis of anisotropy along and across the strike of the fault rupture, and the derivation of IPEs for other fault kinematics.

Author Contributions: M.P., conceptualization, methodology, formal analysis, and preparation of the draft manuscript; F.F., conceptualization, methodology, data validation, and review; P.L., conceptualization, supervision, and review; A.M.M., supervision and writing—review and editing; M.M.V.-B. and S.P., writing—review and editing. All authors have read and approved the published version of the manuscript.

Funding: This research was supported by the European Union—Next Generation EU—Mission 4 "Education and Research"—Component 2 "From Research to Business"—Investment 3.1 "Fund for the realization of an integrated system of research an innovation infrastructure"—Project IR0000037—GeoSciences IR.

Institutional Review Board Statement: Not applicable.

Informed Consent Statement: Not applicable.

Data Availability Statement: The new dataset on the environmental effects caused by the Mw 6.9, 23 November 1980, Irpinia–Basilicata earthquake, Italy is available on Zenodo at https://zenodo.org/records/10277164. Additionally, the new dataset on the environmental effects caused by the Mw Ms 6.7, Mb 6.9, 19 November 1912, Acambay earthquake, Mexico, is available on Zenodo at https://zenodo.org/records/10641336.

Conflicts of Interest: The authors declare no conflicts of interest.

References

1. de Rossi, M.S. Programma dell'osservatorio ed archivio centrale geodinamico presso ii R. Comitato Geologico d'Italia. *Bull. Vulcan. Ital.* **1883**, *10*, 3–128. (In Italian)
2. Mercalli, G. Sulle modificazioni proposte alla scala sismica De Rossi–Forel. *Boll. Soc. Sismol. Ital.* **1902**, *8*, 184–191. (In Italian)
3. Musson, R.M.W.; Griinthal, G.; Stucchi, M. The comparison of macroseismic intensity scales. *J. Seismol.* **2010**, *14*, 413–428. [CrossRef]
4. Gupta, I.N.; Nuttli, O.W. Spatial attenuation of intensities for central US earthquakes. *Bull. Seismol. Soc. Am.* **1976**, *66*, 743–751. [CrossRef]
5. Mak, S.; Clements, R.A.; Schorlemmer, D. Validating intensity prediction equations for Italy by observations. *Bull. Seismol. Soc. Am.* **2015**, *105*, 2942–2954. [CrossRef]
6. Douglas, J. Earthquake ground motion estimation using strong-motion records: A review of equations for the estimation of peak ground acceleration and response spectral ordinates. *Earth-Sci. Rev.* **2003**, *61*, 43–104. [CrossRef]
7. Chandra, U.; McWhorter, J.G.; Nowroozi, A.A. Attenuation of intensities in Iran. *Bull. Seismol. Soc. Am.* **1979**, *69*, 237–250. [CrossRef]
8. Kaila, K.L.; Sarkar, D. Earthquake intensity attenuation pattern in the United States. *Geophys. J. Int.* **1982**, *70*, 31–39. [CrossRef]
9. Lee, K.; Kim, J.K. Intensity attenuation in the Sino-Korean craton. *Bull. Seismol. Soc. Am.* **2002**, *92*, 783–793. [CrossRef]
10. Ferrario, M.F.; Livio, F.; Capizzano, S.S.; Michetti, A.M. Developing the first intensity prediction equation based on the environmental scale intensity: A case study from strong normal-faulting earthquakes in the Italian Apennines. *Seismol. Res. Lett.* **2020**, *91*, 2611–2623. [CrossRef]
11. Michetti, A.M.; Esposito, E.; Guerrieri, L.; Porfido, S.; Serva, L.; Tatevossian, R.; Vittori, E.; Audemard, F.; Azuma, T.; Clague, J.; et al. Environmental seismic intensity scale-ESI 2007. *Bolletino Soc. Geol. Ital.* **2007**, *2*, 11–20.
12. Serva, L.; Vittori, E.; Comerci, V.; Esposito, E.; Guerrieri, L.; Michetti, A.M.; Mohammadioun, B.; Mohammadioun, G.C.; Porfido, S.; Tatevossian, R.E. Earthquake hazard and the Environmental Seismic Intensity (ESI) scale. *Pure Appl. Geophys.* **2016**, *173*, 1479–1515. [CrossRef]
13. Serva, L. History of the Environmental Seismic Intensity Scale ESI-07. *Geosciences* **2019**, *9*, 210. [CrossRef]
14. Lekkas, E.L. The 12 May 2008 Mw 7.9 Wenchuan, China, Earthquake: Macroseismic Intensity Assessment Using the EMS-98 and ESI 2007 Scales and their correlation with the geological structure. *Bull. Seismol. Soc. Am.* **2010**, *100*, 2791–2804. [CrossRef]
15. Sanchez, J.J.; Maldonado, R.F. Application of the ESI 2007 scale to two large earthquakes: South Island, New Zealand (2010 M w 7.1), and Tohoku, Japan (2011 M w 9.0). *Bull. Seismol. Soc. Am.* **2016**, *106*, 1151–1161. [CrossRef]
16. Mavroulis, S.; Argyropoulos, I.; Vassilakis, E.; Carydis, P.; Lekkas, E. Earthquake environmental effects and building properties controlling damage caused by the 6 February 2023 Earthquakes in East Anatolia. *Geosciences* **2023**, *13*, 303. [CrossRef]
17. Schmitt, R.G.; Tanyas, H.; Jessee, M.A.N.; Zhu, J.; Biegel, K.M.; Allstadt, K.E.; Jibson, R.W.; Thompson, E.M.; van Westen, C.J.; Sato, H.P.; et al. *An Open Repository of Earthquake Triggered Ground-Failure Inventories*; U.S. Geological Survey Data Series 1064; U.S. Geological Survey: Reston, VA, USA, 2017.
18. Tanyaş, H.; van Westen, C.J.; Allstadt, K.E.; Anna Nowicki Jessee, M.; Görüm, T.; Jibson, R.W.; Godt, J.W.; Sato, H.P.; Schmitt, R.G.; Odin, M.; et al. Presentation and analysis of a worldwide database of earthquake-induced landslide inventories. *J. Geophys. Res. Earth Surf.* **2017**, *122*, 1991–2015. [CrossRef]
19. Sarmiento, A.; Madugo, D.; Bozorgnia, Y.; Shen, A.; Mazzoni, S.; Lavrentiadis, G.; Dawson, T.; Madugo, C.; Kottke, A.; Thompson, S.; et al. Fault displacement hazard initiative database. In *Fault Displacement Hazard Initiative Database, Report GIRS-2021-08*; Revision 3.3; The B. John Garrick Institute for the Risk Sciences at UCLA Engineering: Los Angeles CA, USA, 2021.
20. Nurminen, F.; Baize, S.; Boncio, P.; Blumetti, A.M.; Cinti, F.R.; Civico, R.; Guerrieri, L. SURE 2.0—New release of the worldwide database of surface ruptures for fault displacement hazard analyses. *Sci. Data* **2022**, *9*, 729. [CrossRef]
21. Bottari, C. Archaeoseismology in Sicily: Past Earthquakes and Effects on Ancient Society. In *Earthquakes and Their Impact on Society*; Springer International Publishing: Cham, Switzerland, 2015; pp. 491–504.
22. Naik, S.P.; Mohanty, A.; Porfido, S.; Tuttle, M.; Gwon, O.; Kim, Y.S. Intensity estimation for the 2001 Bhuj earthquake, India on ESI-07 scale and comparison with historical 16th June 1819 Allah Bund earthquake: A test of ESI-07 application for intraplate earthquakes. *Quat. Int.* **2020**, *536*, 127–143. [CrossRef]

23. Hough, S.E.; Bilham, R. The 1886 Charleston, South Carolina, Earthquake: Intensities and Ground Motions. *Bull. Seismol. Soc. Am.* **2024**, *114*, 1658–1679. [CrossRef]
24. Michetti, A.M.; Esposito, E.; Mohammadioun, B.; Mohammadioun, J.; Gürpinar, A.; Porfido, S.; Rogozhin, E.; Serva, L.; Tatevossian, R.; Vittori, E.; et al. The INQUA scale: An innovative approach for assessing earthquake intensities based on seismically-induced ground effects in the environment. In *Memorie Descrittive della Carta Geologica D'Italia*; Vittori, E., Comerci, V., Eds.; Special paper; INQUA: Rome, Italy, 2004; pp. 1–120.
25. Guerrieri, L.; Tatevossian, R.; Vittori, E.; Comerci, V.; Esposito, E.; Michetti, A.M.; Porfido, S.; Serva, L. Earthquake environmental effects (EEE) and intensity assessment: The INQUA scale project. *Boll. Soc. Geol. Ital.* **2007**, *126*, 375.
26. Papanikolaou, I.D.; Papanikolaou, D.I.; Lekkas, E.L. Advances and limitations of the Environmental Seismic Intensity scale (ESI 2007) regarding near-field and far-field effects from recent earthquakes in Greece: Implications for the seismic hazard assessment. *Geol. Soc. Lond. Spec. Publ.* **2009**, *316*, 11–30. [CrossRef]
27. Bakun, W.H.; Wentworth, C.M. Estimating earthquake location and magnitude from seismic intensity data. *Bull. Seismol. Soc. Am.* **1997**, *87*, 1502–1521. [CrossRef]
28. Gasperini, P.; Bernardini, F.; Valensise, G.; Boschi, E. Defining seismogenic sources from historical earthquake felt reports. *Bull. Seismol. Soc. Am.* **1999**, *89*, 94–110. [CrossRef]
29. Gasperini, P.; Vannucci, G.; Tripone, D.; Boschi, E. The location and sizing of historical earthquakes using the attenuation of macroseismic intensity with distance. *Bull. Seismol. Soc. Am.* **2010**, *100*, 2035–2066. [CrossRef]
30. Bakun, W.H.; Scotti, O. Regional intensity attenuation models for France and the estimation of magnitude and location of historical earthquakes. *Geophys. J. Int.* **2006**, *164*, 596–610. [CrossRef]
31. Gasperini, P. The attenuation of seismic intensity in Italy: A bilinear shape indicates the dominance of deep phases at epicentral distances longer than 45 km. *Bull. Seismol. Soc. Am.* **2001**, *91*, 826–841. [CrossRef]
32. Albarello, D.; D'Amico, V. Attenuation relationship of macroseismic intensity in Italy for probabilistic seismic hazard assessment. *Boll. Geofis. Teor. Ed. Appl.* **2004**, *45*, 271–284.
33. Kaklamanos, J.; Baise, L.G.; Boore, D.M. Estimating unknown input parameters when implementing the NGA ground-motion prediction equations in engineering practice. *Earthq. Spectra* **2011**, *27*, 1219–1235. [CrossRef]
34. Allen, T.I.; Wald, D.J.; Worden, C.B. Intensity attenuation for active crustal regions. *J. Seismol.* **2012**, *16*, 409–433. [CrossRef]
35. Chunga, K.; Livio, F.; Mulas, M.; Ochoa-Cornejo, F.; Besenzon, D.; Ferrario, M.F.; Michetti, A.M. Earthquake ground effects and intensity of the 16 April 2016 Mw 7.8 Pedernales, Ecuador, earthquake: Implications for the source characterization of large subduction earthquakes. *Bull. Seismol. Soc. Am.* **2018**, *108*, 3384–3397. [CrossRef]
36. Rovida, A.; Locati, M.; Camassi, R.; Lolli, B.; Gasperini, P.; Antonucci, A. *Catalogo Parametrico dei Terremoti Italiani (CPTI15)*; versione 4.0; Istituto Nazionale di Geofisica e Vulcanologia (INGV): Roma, Italy, 2022. [CrossRef]
37. Serva, L.; Esposito, E.; Guerrieri, L.; Porfido, S.; Vittori, E.; Comerci, V. Environmental effects from five historical earthquakes in southern Apennines (Italy) and macroseismic intensity assessment: Contribution to INQUA EEE Scale Project. *Quat. Int.* **2007**, *173*, 30–44. [CrossRef]
38. Pizza, M.; Ferrario, M.F.; Michetti, A.L.; Nappi, R.; Velázquez-Bucio, M.M.; Lacan, P.; Porfido, S. Environmental effects caused by the Mw 6.9 23 November 1980 Irpinia-Basilicata Earthquake, Italy. Zenodo. 2023. Available online: https://zenodo.org/records/10277164 (accessed on 26 February 2024).
39. Guerrieri, L.; Blumetti, A.M.; Brustia, E.; Esposito, E.; Lucarini, M.; Michetti, A.M.; Porfido, S.; Serva, L.; Vittori, E.; Inqua Terpro, group. Earthquake environmental effects, intensity and seismic hazard assessment: The EEE catalogue (Inqua project# 0418). In Proceedings of the 2nd INQUA-IGCP-567 International Workshop on Active Tectonics, Earthquake Geology, Archaeology and Engineering, Corinth, Greece, 19–24 September 2011; pp. 62–65.
40. Nappi, R.; Gaudiosi, G.; Alessio, G.; De Lucia, M.; Porfido, S. The environmental effects of the 1743 Salento earthquake (Apulia, southern Italy): A contribution to seismic hazard assessment of the Salento Peninsula. *Nat. Hazards* **2017**, *86*, 295–324. [CrossRef]
41. Giner-Robles, J.L.; Silva, P.G.; Elez, J.; Rodríguez-Pascua, M.A.; Perez-Lopez, R.; Rodríguez-Escudero, E. Relationships between the ESI-07 scale and expected PGA values from the analysis of two historical earthquakes (≥VIII EMS) in East Spain: Tavernes 1396 AD and Estubeny 1748 AD events. In Proceedings of the 6th International INQUA Meeting in Paleoseismology, Active Tectonics and Archaeoseismology, Pescina, Italy, 19–24 April 2015; pp. 19–24.
42. Blumetti, A.M.; Guerrieri, L.; Porfido, S. Cataloguing the EEEs induced by the 1783 5th February Calabrian earthquake: Implications for an improved seismic hazard. In *Earthquake Environmental Effect for Seismic Hazard Assessment: The ESI Intensity Scale and the EEE Catalogue*; Memorie descrittive della Carta geologica d'Italia-VOLUME XCVII Chapter: 4.4 Cataloguing the EEEs induceded by the 1783 5th FebruaryPublisher: A.T.I.-SYSTEMCART srl-S.EL.CA. srl.; Guerrieri, L., Ed.; ISPRA-Servizio Geologico d'Italia: Roma, Italy, 2015; p. 97.
43. Papanikolaou, I.; Melaki, M. The Environmental Seismic Intensity Scale (ESI 2007) in Greece, addition of new events and its relationship with magnitude in Greece and the Mediterranean; preliminary attenuation relationships. *Quat. Int.* **2017**, *451*, 37–55. [CrossRef]
44. Comerci, V.; Vittori, E.; Blumetti, A.M.; Brustia, E.; Di Manna, P.; Guerrieri, L.; Lucarini, M.; Serva, L. Environmental effects of the December 28, 1908, Southern Calabria–Messina (Southern Italy) earthquake. *Nat. Hazards* **2015**, *76*, 1849–1891. [CrossRef]
45. Velázquez-Bucio, M.M.; Lacan, P.; Pizza, M.; Ferrario, M.F.; Porfido, S.; Michetti, A.M. Environmental Effects Caused By The Ms 6.7, Mb 6.9, November 19th, 1912, Acambay Earthquake, Mexico. Zenodo. 2024. Available online: https://zenodo.org/records/10641336 (accessed on 28 February 2024).

46. Papathanassiou, G.; Valkaniotis, S.; Pavlides, S. Applying the INQUA scale to the Sofades 1954, Central Greece, earthquake. *Bull. Geol. Soc. Greece* **2007**, *40*, 1226–1233. [CrossRef]
47. Silva, P.G.; Rodríguez-Pascua, M.A.; Giner-Robles, J.L.; Pérez-López, R.; Lario, J.; Perucha, M.A.; Bardají, T.; Huerta, P.; Roquero, E.; Bautista Davila, M.B. *Catálogo de los Efectos Geológicos de los Terremotos de*, España 1ª ed; Riesgos Geológicos y Geotecnia 4; IGME: Madrid, Spain, 2014; p. 352.
48. Fountoulis, I.G.; Mavroulis, S.D. Application of the Environmental Seismic Intensity scale (ESI 2007) and the European Macroseismic Scale (EMS-98) to the Kalamata (SW Peloponnese, Greece) earthquake (Ms = 6.2, September 13, 1986) and correlation with neotectonic structures and active faults. *Ann. Geophys.* **2013**, *56*, S0675.
49. Mavroulis, S.; Triantafyllou, I.; Karavias, A.; Gogou, M.; Katsetsiadou, K.N.; Lekkas, E.; Papadopoulos, G.A.; Parcharidis, I. Primary and secondary environmental effects triggered by the 30 October 2020, Mw = 7.0, Samos (Eastern Aegean Sea, Greece) earthquake based on post-event field surveys and InSAR analysis. *Appl. Sci.* **2021**, *11*, 3281. [CrossRef]
50. Langridge, R.M.; Weldon, R.J.; Moya, J.C.; Suárez, G. Paleoseismology of the 1912 Acambay earthquake and the Acambay-Tixmadejé fault, Trans-Mexican volcanic belt. *J. Geophys. Res. Solid Earth* **2000**, *105*, 3019–3037. [CrossRef]
51. Rodríguez-Pascua, M.A.; Pérez-López, R.; Garduño-Monroy, V.H.; Perucha, M.A.; Israde-Alcántara, I. Estimation of the epicentral area of the 1912 Acambay earthquake (M 6.9, Mexico) determined from the earthquake archaeological effects (EAE) and the ESI07 macroseismic scale. *Quat. Int.* **2017**, *451*, 74–86. [CrossRef]
52. Pantosti, D.; De Martini, P.M.; Papanastassiou, D.; Palyvos, N.; Lemeille, F.; Stavrakakis, G. A reappraisal of the 1894 Atalanti earthquake surface ruptures, central Greece. *Bull. Seismol. Soc. Am.* **2001**, *91*, 760–780. [CrossRef]
53. Pantosti, D.; Valensise, G. Source geometry and long term behavior of the 1980, Irpinia earthquake fault based on field geologic observations. *Ann. Geophys.* **1993**, *36*. [CrossRef]
54. Michetti, A.M.; Brunamonte, F.; Serva, L.; Vittori, E. Trench investigations of the 1915 Fucino earthquake fault scarps (Abruzzo, Central Italy): Geological evidence of large historical events. *J. Geophys. Res. Solid Earth* **1996**, *101*, 5921–5936. [CrossRef]
55. Cello, G.; Deiana, G.; Mangano, P.; Mazzoli, S.; Tondi, E.; Ferreli, L.; Maschio, L.; Michetti, A.M.; Serva, L.; Vittori, E. Evidence for surface faulting during the September 26, 1997, Colfiorito (Central Italy) earthquakes. *J. Earthq. Eng.* **1998**, *2*, 303–324. [CrossRef]
56. Mountrakis, D.; Pavlides, S.; Zouros, N.; Astaras, T.; Chatzipetros, A. Seismic fault geometry and kinematics of the 13 May 1995 Western Macedonia (Greece) earthquake. *J. Geodyn.* **1998**, *26*, 175–196. [CrossRef]
57. Tranos, M.D.; Papadimitriou, E.E.; Kilias, A.A. Thessaloniki–Gerakarou Fault Zone (TGFZ): The western extension of the 1978 Thessaloniki earthquake fault (Northern Greece) and seismic hazard assessment. *J. Struct. Geol.* **2003**, *25*, 2109–2123. [CrossRef]
58. Vittori, E.; Di Manna, P.; Blumetti, A.M.; Comerci, V.; Guerrieri, L.; Esposito, E.; Michetti, A.M.; Porfido, S.; Piccardi, L.; Roberts, G.P.; et al. Surface faulting of the 6 April 2009 Mw 6.3 L'Aquila earthquake in Central Italy. *Bull. Seismol. Soc. Am.* **2011**, *101*, 1507–1530. [CrossRef]
59. Livio, F.A.; Michetti, A.M.; Vittori, E.; Gregory, L.; Wedmore, L.; Piccardi, L.; Tondi, E.; Roberts, G.P.; Blumetti, A.M.; Bonadeo, L.; et al. Surface faulting during the August 24, 2016, Central Italy earthquake (Mw 6.0): Preliminary results. *Ann. Geophys.* **2016**, *59*.
60. Hough, S.E. Missing great earthquakes. *J. Geophys. Res. Solid Earth* **2013**, *118*, 1098–1108. [CrossRef]
61. Seal, D.M.; Jessee, A.N.; Hamburger, M.W.; Dills, C.W.; Allstadt, K.E. Comprehensive Global Database of Earthquake-Induced Landslide Events and Their Impacts (ver. 2.0, February 2022): US Geological Survey Data Release. 2022. Available online: https://www.sciencebase.gov/catalog/item/614512b3d34e0df5fb95b5f9 (accessed on 27 May 2024).
62. Grandori, G.; Drei, A.; Perotti, F.; Tagliani, A. Macroseismic intensity versus epicentral distance: The case of Central Italy. *Tectonophysics* **1991**, *193*, 165–171. [CrossRef]
63. Berardi, R.; Petrungaro, C.; Zonetti, L.; Magri, L.; Mucciarelli, M. *Mappe di Sismicità per l'area Italiana*; Technical Report; ISMES/ENEL: Golden, CO, USA, 1993; Volume 51.
64. Pasolini, C.; Albarello, D.; Gasperini, P.; D'Amico, V.; Lolli, B. The attenuation of seismic intensity in Italy, Part II: Modeling and validation. *Bull. Seismol. Soc. Am.* **2008**, *98*, 692–708. [CrossRef]
65. Gómez-Capera, A.A.; D'Amico, V.; Meletti, C.; Rovida, A.; Albarello, D. Seismic hazard assessment in terms of macroseismic intensity in Italy: A critical analysis from the comparison of different computational procedures. *Bull. Seismol. Soc. Am.* **2010**, *100*, 1614–1631. [CrossRef]
66. Gomez-Capera, A.A.; Santulin, M.; D'Amico, M.; D'Amico, V.; Locati, M.; Meletti, C.; Varini, E. Macroseismic intensity attenuation models calibrated in Mw for Italy. *Bull. Earthq. Eng.* **2024**, *22*, 795–843. [CrossRef]
67. Vannucci, G.; Lolli, B.; Gasperini, P. A theoretical comparison among macroseismic scales used in Italy. *Bull. Earthq. Eng.* **2024**, *22*, 4245–4263. [CrossRef]
68. Wells, D.L.; Coppersmith, K.J. New empirical relationships among magnitude, rupture length, rupture width, rupture area, and surface displacement. *Bull. Seismol. Soc. Am.* **1994**, *84*, 974–1002. [CrossRef]
69. McGuire, R.K. Computations of seismic hazard. *Ann. Geophys.* **1993**, *36*. [CrossRef]
70. Papanikolaou, I.D. Uncertainty in intensity assignment and attenuation relationships: How seismic hazard maps can benefit from the implementation of the Environmental Seismic Intensity scale (ESI 2007). *Quat. Int.* **2011**, *242*, 42–51. [CrossRef]